International Refereed Journal of Engineering and Science (IRJES)
ISSN (Online) 2319-183X, (Print) 2319-1821
Volume 15, Issue 4 (Jul. – Aug. 2026), PP. 118-129

Fuzzy-Supervised PID Speed Regulation of a Hydropower Generator in an Isolated Hydro-Photovoltaic System

Duy-Trung Nguyen[1], Quang-Hue Dam[2], N.-K Nguyen[1,*]
[1]*Faculty of Automation, Artificial Intelligence, and Intelligent Systems,*
Electric Power University, Hanoi, Vietnam
[2]*Practice and Experiment Center, Electric Power University, Hanoi, Vietnam*
**Corresponding Author: nknresearch@gmail.com*

Abstract: *High levels of photovoltaic generation reduce water consumption in an isolated hydroelectric system, but the net-load ramps produced are challenging in reconciling fixed governor gains with hydraulic lag, wicket-gate limits, and low system inertia. A bounded fuzzy-supervised proportional-integral-derivative (FSPID) governor is proposed in this paper. The underlying PID law includes derivative filtering, conditional anti-windup, and explicit gate saturation. The proportional, integral, and derivative gains are scheduled by fuzzy inference from normalized frequency error and filtered error rate. A nonlinear reduced order hydro-PV model is compared to PI, fixed PID and a direct fuzzy-PID baseline. Four 120-s cases are presented with deterministic load and irradiance steps, stochastic load-solar variation, severe parameter sensitive ramps and a PV outage with load growth. A 30 run Monte Carlo test is also performed varying the inertia, turbine time constant, load damping and measurement noise. In all the deterministic cases, the proposed controller provides the minimum IAE, ISE, ITSE, ITAE and peak frequency deviation. The mean ITAE for parameter-uncertainty study is 134.86. PI, PID and fuzzy-PID are 189.57, 151.60, 149.34, respectively. The results support bounded fuzzy gain supervision as a feasible improvement to the conventional hydro governor. The conclusions are specific to the model and the uncertainty domain.*

Keywords: *hydropower governor, isolated grid, photovoltaic generation, fuzzy supervision, PID gain scheduling, frequency control, Monte Carlo analysis*

Date of Submission: 15-08-2026 Date of acceptance: 31-08-2026

I. INTRODUCTION

Frequency regulation becomes ruthless when a local grid is disconnected from a large interconnected system. The synchronous hydropower generator must then balance demand, PV injection and its own hydraulic constraints with little external inertial support. Field tests performed on an isolated power plant have shown that the governor stability is very sensitive to the PID tuning [1]. A similar conclusion can be made for studies of hydro-supported renewable islands, where the controllable hydro unit takes most of the power mismatch caused by weather dependent generation and the dynamics of the waterway have a strong influence on the amount of bandwidth that can be obtained [2].

Three directions have been followed in recent load-frequency-control research. The first one improves the tuning of PID-type regulators for islanded microgrids [3]-[4]. The latter are fuzzy, fractional-order or adaptive layers which compensate the variation of operating-point [5]-[11]. The third approach is based on robust, predictive, reinforcement learning or metaheuristic control for nonlinear hydro and renewable rich systems [12]-[22]. Since 2022 reviews agree that it is better to analyze renewable variability, less inertia, practical non-linearities and uncertainty in combination instead of relying on a single nominal load step [23], [24].

More discussion is needed about hydro-PV systems. A hydropower unit can change the mechanical power rapidly but the wicket gate, water column and turbine do not respond instantaneously. Fast gain selection can excite an adverse mode of the waterway. Long tail of frequency for conservative gains. Hence, the recent studies on hydro-governors were focused on the nonlinear robust control, governor optimization, sliding modes, internal-model control, and fuzzy PID adaptation [14]-[22], [25]-[32]. In 2024, a hydro-PV study showed the value of data-driven optimal control, but with a different structure and training requirements for an industrial PID governor [33]. More recent work on adaptive hydro PID, generalized-inverse internal-model control, hydro-wind-solar-storage regulation and fuzzy control of isolated renewable systems confirms the move to bounded online adaptation [34]-[37].

Here the filled gap is narrower and practical. Many intelligent LFC papers provide a single objective index, do not allow unequal actuator authority across controllers, or do not provide code to reproduce their plots. Some fuzzy-PID schemes directly output the actuator command, which obscures the relation with existing governor protection logic. But in the present design the fuzzy logic is used only as a bounded gain supervisor. The PID core, the saturation, the derivative filter, and the conditional integrator are still visible. The comparison is done on equal footing, PI, PID, fuzzy-PID and FSPID are provided with the same measurements, limits, sampling interval, disturbances, and initial states.

There are four contributions in this paper. First, a compact nonlinear hydro-PV frequency model is developed, which includes explicit power balance, turbine lag, nonlinear hydraulic loss and gate limits. Second, it establishes a two-input supervisor, with analytically bounded proportional, integral and derivative gains. Third, it has an uncertainty study with 30 runs and four disturbance cases which are evaluated with peak frequency deviation, IAE, ISE, ITSE and ITAE. Finally, a flowchart for application of the MATLAB software for the simulation is provided. The claims are purposely narrow because the study defines comparative performance within the modeled envelope, not universal plant-level stability.

II. MATHEMATICAL MODEL AND TEST SYSTEM

A. Hydro-PV isolated-grid structure

The considered architecture is shown in Figure 1. The speed reference signal is compared with the measured frequency of the generator. The obtained error is fed to the Fuzzy gain supervisor, and constrained PID law. The feedback path begins at the measured-frequency output node and feeds back to the summing junction (not connected to the PV or load branches) with straight orthogonal segments. PV power and load demand are exogenous terms in the generator-load balance.

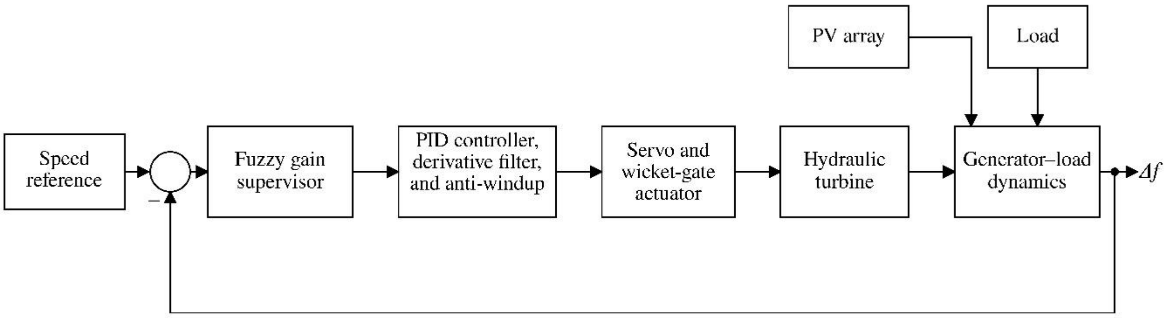

Fig. 1. Corrected closed-loop architecture of the isolated hydro-PV system.

The instantaneous active-power mismatch and the per-unit swing relation are given by (1) and (2), respectively.

$$\Delta P(t) = P_m(t) + P_{PV}(t) - P_L(t) \quad (1)$$

$$2H\frac{d\Delta f(t)}{dt} = \Delta P(t) - D\Delta f(t) \quad (2)$$

Turbine mechanical power, PV injection, load demand, aggregate inertia, load damping, and frequency deviation are the terms used in (1) and (2), respectively. The generator accelerates when there is a positive power mismatch. The MATLAB implementation maintains this sign convention.

B. Servo, turbine, and PV representations

The wicket-gate servo and reduced nonlinear turbine are described by (3) and (4). The saturation operator enforces the same physical opening limits for every controller.

$$T_s\frac{dy(t)}{dt} + y(t) = \mathrm{sat}_{[y_{\min},y_{\max}]}[u(t)] \quad (3)$$

$$T_t\frac{dP_m(t)}{dt} = y(t) - P_m(t) - k_n P_m(t)|P_m(t)| \quad (4)$$

The final nonlinear term in (4) is a compact representation of operating-point-dependent hydraulic loss. It is not a substitute for an elastic water-hammer model. PV power follows (5); in the numerical tests, irradiance is imposed directly so that every controller experiences an identical renewable-power trajectory.

$$P_{PV}(t) = P_{PV,r}\frac{G(t)}{G_r}[1 + \gamma_T(T_c(t) - T_r)] \quad (5)$$

The parameters used throughout the study are collected in Table 1. Table 1 is also the single source of nominal values used in the simulation process executed in MATLAB software.

Table 1. Nominal model and simulation parameters

Quantity	Symbol	Value	Unit
Inertia constant	H	3.50	s
Load damping	D	1.10	p.u./p.u.
Servo time constant	T_s	0.28	s
Turbine time constant	T_t	1.35	s
Hydraulic-loss coefficient	k_n	0.08	p.u.−1
Rated PV injection	$P_{PV,r}$	0.22	p.u.
Gate limits	u_{min}, u_{max}	0.08, 0.95	p.u.
Derivative-filter constant	T_f	0.08	s
Integration step	Δt	0.01	s

Table 2 positions the model against recent work. The purpose is not to claim a higher-fidelity waterway representation than specialized hydro models. Rather, the proposed benchmark adds reproducible uncertainty and multi-event evaluation to a transparent governor structure.

Table 2. Control-oriented relationship to recent studies

Study group	Representative refs.	Main strength	Gap addressed here
Islanded PID/fuzzy LFC	[3]-[11]	Simple or adaptive frequency control	Common limits and four integral indices
Nonlinear hydro control	[12]-[22], [25]-[30]	Detailed robustness or optimization	Transparent bounded PID supervision
Hydro-PV optimal control	[31]	Data-driven optimal policy	Industrial PID-compatible architecture
Recent LFC reviews	[23], [24]	Broad method taxonomy	Fully reproducible hydro-PV cases

III. BOUNDED FUZZY-SUPERVISED PID

A. PID core and supervisory inputs

The error and its filtered rate are defined in (6). Filtering is essential because an unfiltered derivative would convert measurement noise into rapid gate motion.

$$e(t) = f_{ref} - f(t), \qquad T_f \frac{d\dot{e}_f(t)}{dt} + \dot{e}_f(t) = \dot{e}(t) \tag{6}$$

The unconstrained and constrained controller outputs follow (7) and (8). Conditional integration stops the integral state when saturation and the error sign would push the command farther outside the admissible interval.

$$u_0(t) = u_{eq} + K_p(t)e(t) + K_i(t)\int_0^t e\,(\tau)d\tau + K_d(t)\dot{e}_f(t) \tag{7}$$

$$u(t) = \mathrm{sat}_{[u_{\min},u_{\max}]}[u_0(t)] \tag{8}$$

B. Fuzzy interpolation and gain bounds

Normalized supervisor inputs are given by (9). Low, medium, and high triangular membership functions are used. Their centroid-equivalent interpolation is summarized by q in (10), followed by the scheduled gains in (11).

$$e_n = \min(1, K_e|e|), \qquad d_n = \min\left(1, K_d^{(n)}|\dot{e}_f|\right) \tag{9}$$

$$q = 0.62e_n + 0.38d_n \tag{10}$$

$$K_p = K_{p0}(0.88 + 0.62q), \quad K_i = K_{i0}(1.22 - 0.62q), \quad K_d = K_{d0}(0.75 + 0.90d_n) \tag{11}$$

Equation (11) puts an explicit limit on each scheduled gain in terms of its nominal value. Therefore, fuzzy inference cannot get around the declared gain box. Table 3 illustrates the linguistic intent The error rate is high, thus the derivative action increases. When the error itself is large, proportional action increases, and integral action is reduced. Authority integral is recovered near the equilibrium.

The online sequence is shown in Fig. 2. As shown, Fig. 2 distinguishes the inference step from the PID action, actuator constraints, plant integration, and index accumulation. This separation is important for implementation and for later code verification.

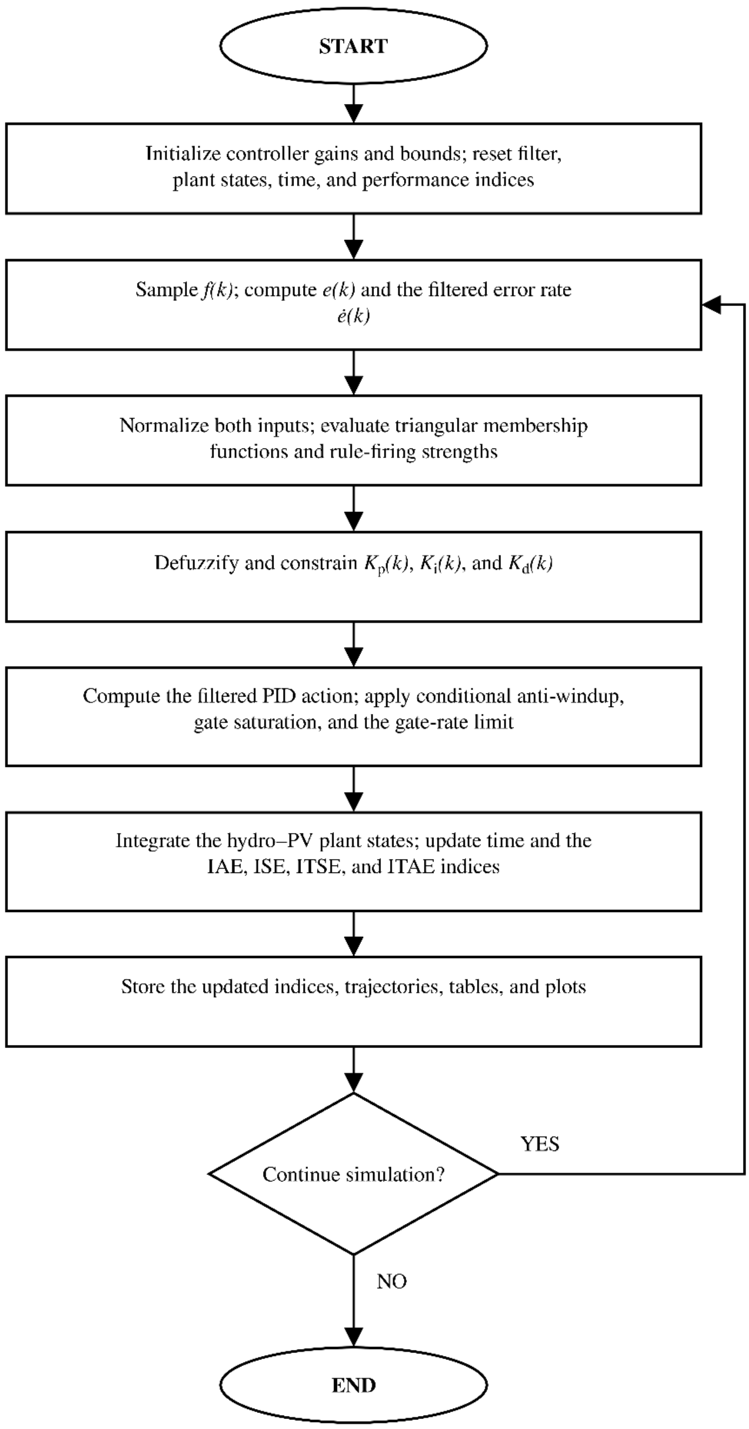

Fig. 2. Online implementation sequence of the proposed FSPID governor.

Table 3. Linguistic rule intent of the gain supervisor

Error level	Filtered-rate level	Proportional correction	Integral correction	Derivative correction

Error level	Filtered-rate level	Proportional correction	Integral correction	Derivative correction
Low	Low	Low	High	Low
Low	High	Medium	Medium	High
Medium	Low	Medium	Medium	Medium
Medium	High	High	Low	High
High	Low	High	Low	Medium
High	High	High	Low	High

For each frozen gain triple, local linearized stability can be checked from the closed-loop eigenvalues. Because the supervisor is time varying and the plant contains saturation, that frozen-gain test alone is not a global proof. This paper therefore avoids a global asymptotic-stability claim. The uncertainty results in Section IV support practical robustness only for the parameter box and disturbances explicitly tested.

IV. SIMULATION RESULTS AND DISCUSSION

A. Cases, controller settings, and indices

Four cases are used. Their definitions appear in Table 4, and their actual load and PV trajectories are plotted in Fig. 3. This pairing prevents a vague description such as "random disturbance" from concealing the applied signal. Case 1 preserves the original load/PV sequence. Case 2 introduces reproducible stochastic variations. Case 3 combines deeper solar ramps with larger demand steps. Case 4 removes PV completely and simultaneously raises demand before partial solar recovery.

Table 4. Simulation cases applied identically to all controllers

Case	Load disturbance	PV/irradiance disturbance	Purpose
1	+0.10 at 20 s; −0.06 at 55 s; +0.08 at 85 s	−45% at 38-52 s; −25% at 75-92 s	Nominal multi-event test
2	Step, sinusoid, and filtered random component	Bounded filtered random irradiance	Continuous variability
3	+0.12 at 25 s; −0.08 at 70 s; +0.10 at 95 s	−55% at 42-68 s; −30% at 88-108 s	Severe ramps
4	+0.15 at 30 s; +0.08 at 72 s	PV trip at 40 s; 70% recovery at 78 s	Generation contingency

Table 5. Controller settings used in every case

Controller	Proportional	Integral	Derivative	Adaptation
PI	1.15	0.32	0	None
PID	1.45	0.42	0.20	None
Fuzzy-PID	1.45	0.42	0.20	Single activation surface
Proposed FSPID	1.75	0.40	0.30	Bounded two-input surface

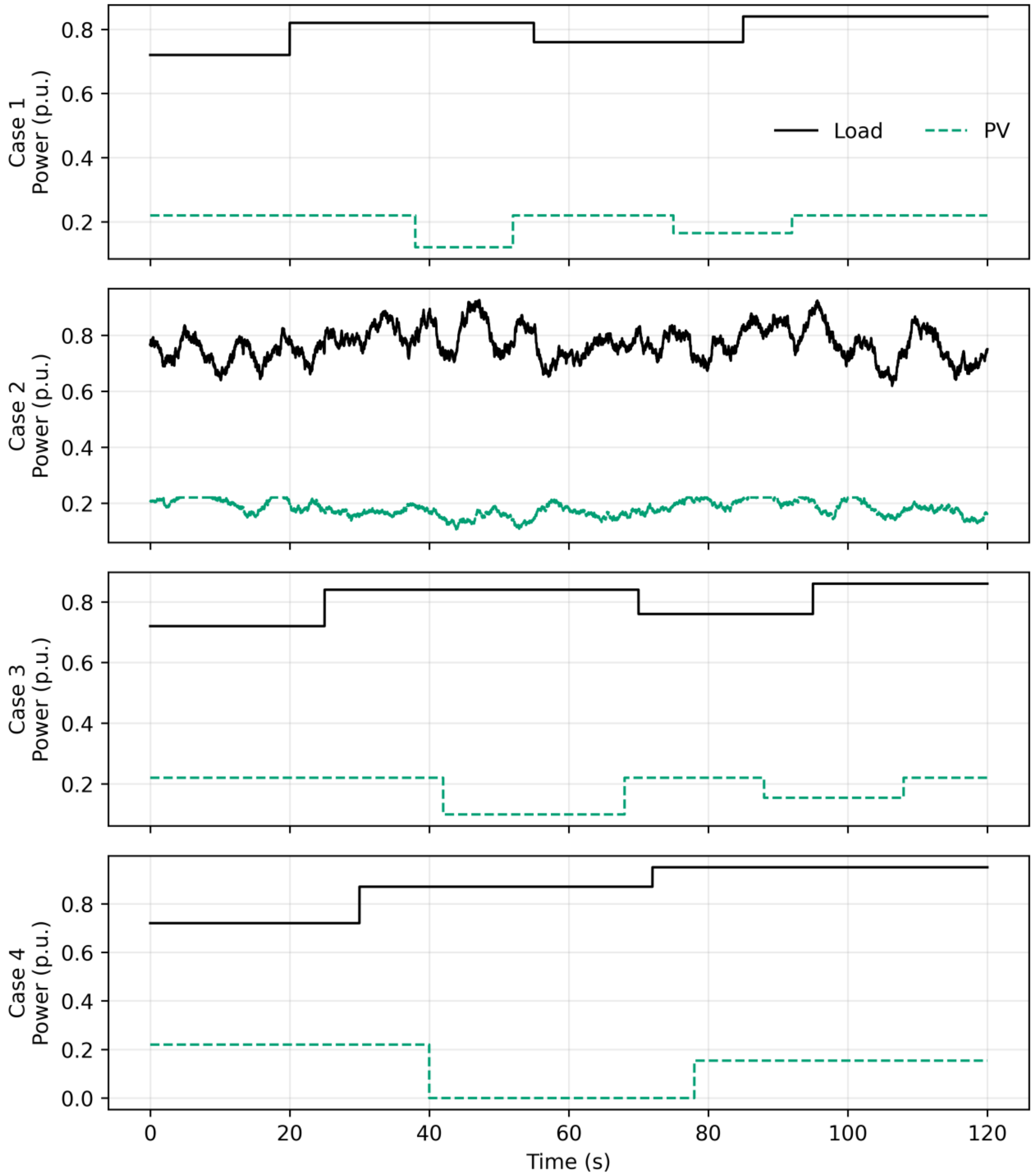

Fig. 3. Load and PV trajectories used in the four simulation cases.

The nominal settings in Table 5 were selected once and then held fixed. Table 5 also shows that the proposed controller is not given a different actuator model or sampling rate.

Performance is assessed by (12) and (13). IAE measures total absolute deviation; ISE emphasizes large peaks; ITSE penalizes large errors that persist late; ITAE highlights long-lived absolute error. Percentage improvement is computed with (14), not by reading approximate values from plots.

$$\mathrm{IAE} = \int_0^T |e(t)|\, dt, \qquad \mathrm{ISE} = \int_0^T e^2\,(t) dt \tag{12}$$

$$\mathrm{ITSE} = \int_0^T t\, e^2(t) dt, \qquad \mathrm{ITAE} = \int_0^T t\, |e(t)| dt \tag{13}$$

$$\rho_j = 100 \frac{J_{j,\mathrm{base}} - J_{j,\mathrm{FSPID}}}{J_{j,\mathrm{base}}}\ (\%), \tag{14}$$

$j \in \{\text{IAE}, \text{ISE}, \text{ITSE}, \text{ITAE}\}$

B. Frequency and control responses

The frequency trajectories are shown in Fig. 4. FSPID has the lowest peak and the fastest damping in all cases. The advantage is small in the continuously varying Case 2 which is scientifically plausible: no controller can force the frequency to zero while net power is continuously wandering without additional storage or PV reserve. In Cases 3 and 4 the advantage becomes more clear, where the supervisor increases proportional and derivative authority at the disturbance edges and reduces integral accumulation during saturation-prone intervals.

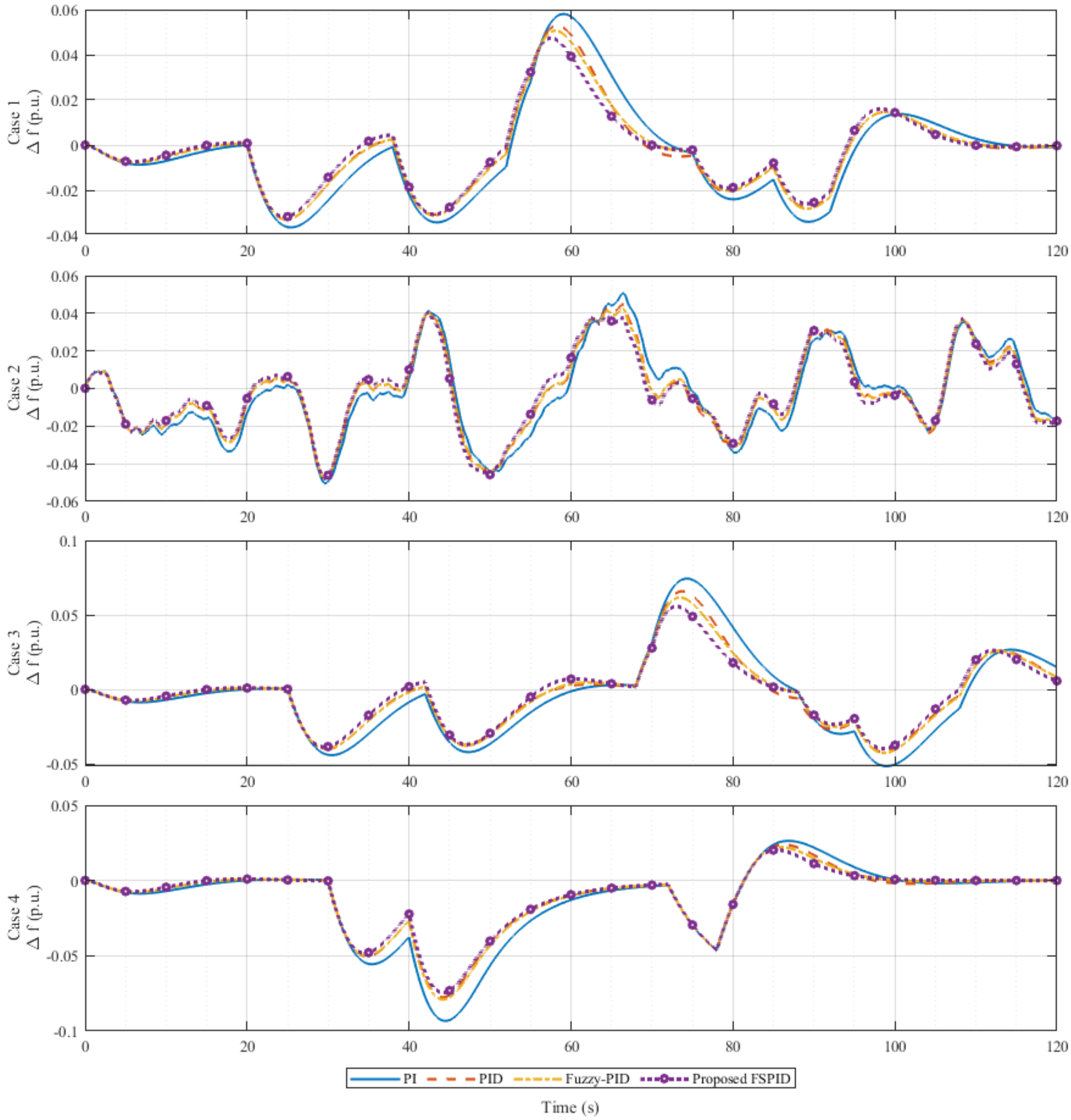

Fig. 4. Frequency deviation for PI, PID, fuzzy-PID, and proposed FSPID in Cases 1-4.

Figure 5 examines the severe contingency in more detail. The gate remains within 0.08-0.95 p.u. for all controllers. The scheduled gains change smoothly rather than switching between discrete values. Hence, the smaller frequency excursion is not obtained by exceeding the common actuator range.

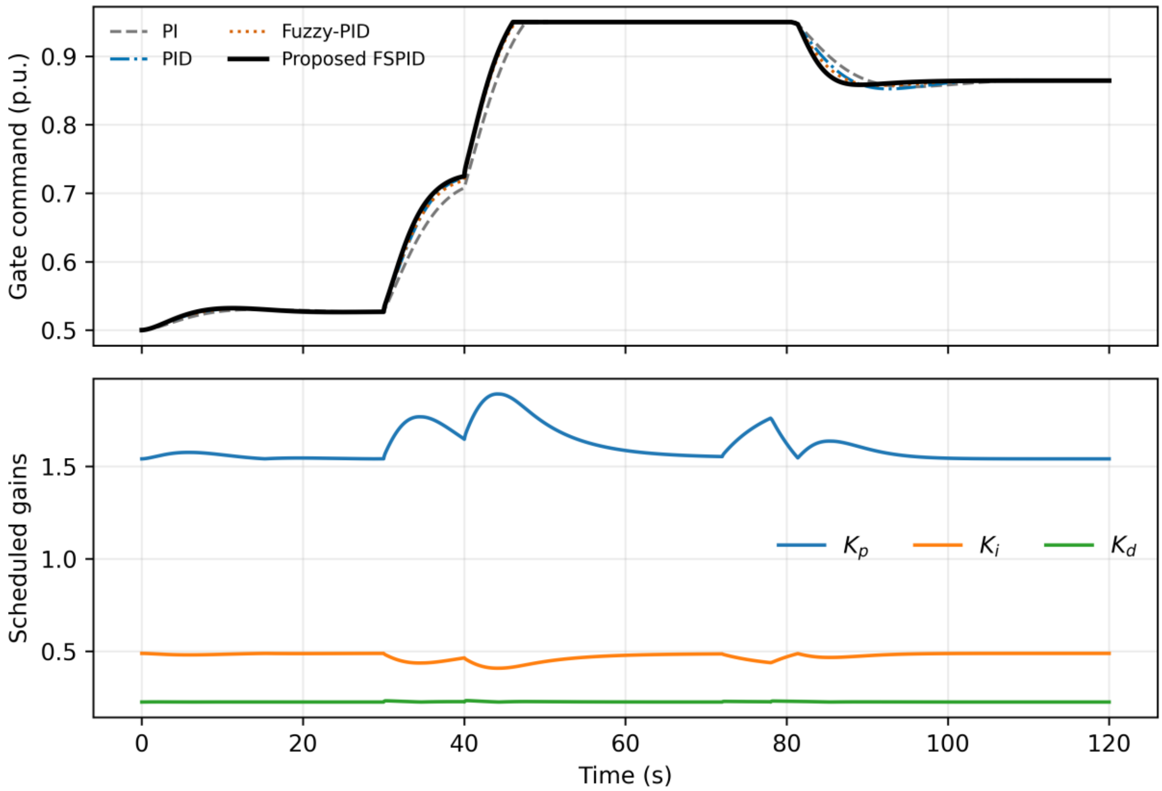

Fig. 5. Gate commands and scheduled FSPID gains in the PV-outage case.

C. Integral indices and uncertainty assessment

Table 6 reports the complete numerical results. The proposed method is lowest in all five measures for all four cases. For example, in Case 3 its ITAE is 132.74, compared with 186.63 for PI, 149.10 for PID, and 146.99 for fuzzy-PID. In Case 4, the corresponding values are 88.47, 116.59, 96.35, and 95.21. These are not isolated improvements in peak value; IAE, ISE, and ITSE move in the same direction.

Table 6. Numerical performance for all cases

Case	Controller	IAE	ISE	ITSE	ITAE	Peak |Δf|
1	PI	1.9918	0.05820	3.3372	115.59	0.05803
	PID	1.6225	0.04146	2.3382	94.00	0.05288
	Fuzzy-PID	1.6061	0.04030	2.2695	92.74	0.05065
	FSPID	1.4734	0.03474	1.9389	84.76	0.04738
2	PI	2.0279	0.05141	3.2698	127.56	0.05183
	PID	1.9081	0.04478	2.9741	123.19	0.04858
	Fuzzy-PID	1.8736	0.04314	2.8394	120.41	0.04782
	FSPID	1.8391	0.04085	2.7254	118.98	0.04691
3	PI	2.6417	0.10125	7.3390	186.63	0.07437
	PID	2.1127	0.06920	4.9468	149.10	0.06585
	Fuzzy-PID	2.0917	0.06603	4.6977	146.99	0.06167
	FSPID	1.9017	0.05491	3.8625	132.74	0.05571
4	PI	2.2025	0.10660	5.1623	116.59	0.09328
	PID	1.8189	0.07330	3.5843	96.35	0.07763
	Fuzzy-PID	1.8187	0.07503	3.6452	95.21	0.07901
	FSPID	1.6972	0.06637	3.2287	88.47	0.07444

Figure 6 normalizes the same values by the PI result in each case. It makes the cross-case pattern visible without hiding the absolute numbers given in Table 6. FSPID reduces the Case 1 indices by 26.0%, 40.3%, 41.9%, and 26.7% relative to PI. Under the PV outage of Case 4, the reductions are 22.9%, 37.7%, 37.5%, and 24.1%.

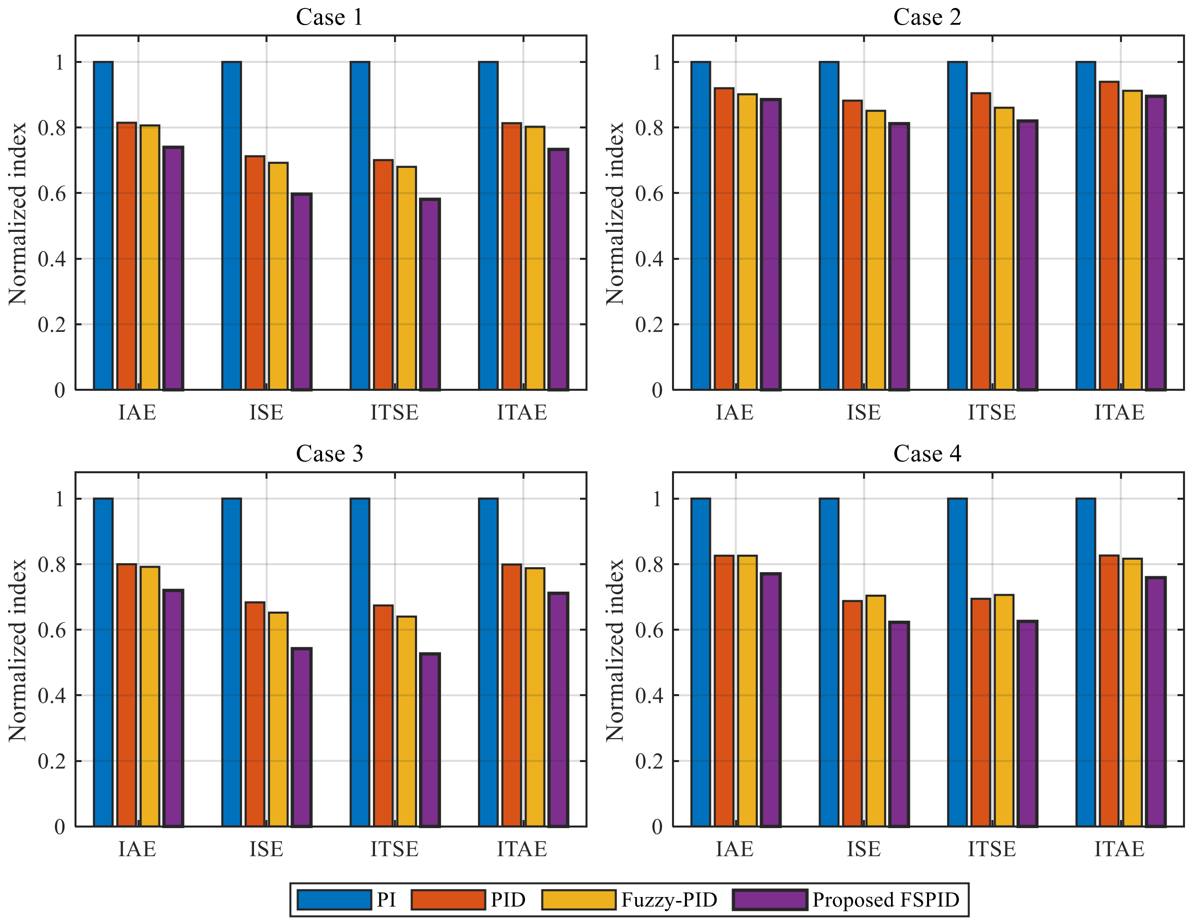

Fig. 6. IAE, ISE, ITSE, and ITAE normalized by the PI result in each case.

For the Monte Carlo experiment, the parameter vector and its uncertainty box are defined in (15). Thirty runs also include frequency-measurement noise with a standard deviation of 2×10−4 p.u. The same sampled plant is used for all four controllers within a run.

$$\boldsymbol{\theta} = [H\ T_t\ D]^{\mathrm{T}}, \quad \boldsymbol{\theta} \in [0.8,1.2]H_0 \times [0.8,1.25]T_{t0} \times [0.85,1.15]D_0 \tag{15}$$

Table 7 summarizes the distribution, while Fig. 7 shows the complete ITAE spread. FSPID lowers mean ITAE by 28.9% relative to PI, 11.0% relative to fixed PID, and 9.7% relative to fuzzy-PID. Its standard deviation is also the smallest. The boxplot does not prove robustness outside the sampled domain, but it shows that the nominal ranking is not destroyed by moderate model uncertainty.

Table 7. Thirty-run uncertainty results for Case 3

Controller	Mean ITAE	Std. ITAE	Mean peak |Δf|
PI	189.572	10.069	0.07429
PID	151.596	8.289	0.06565
Fuzzy-PID	149.340	7.565	0.06154
Proposed FSPID	134.860	6.748	0.05553

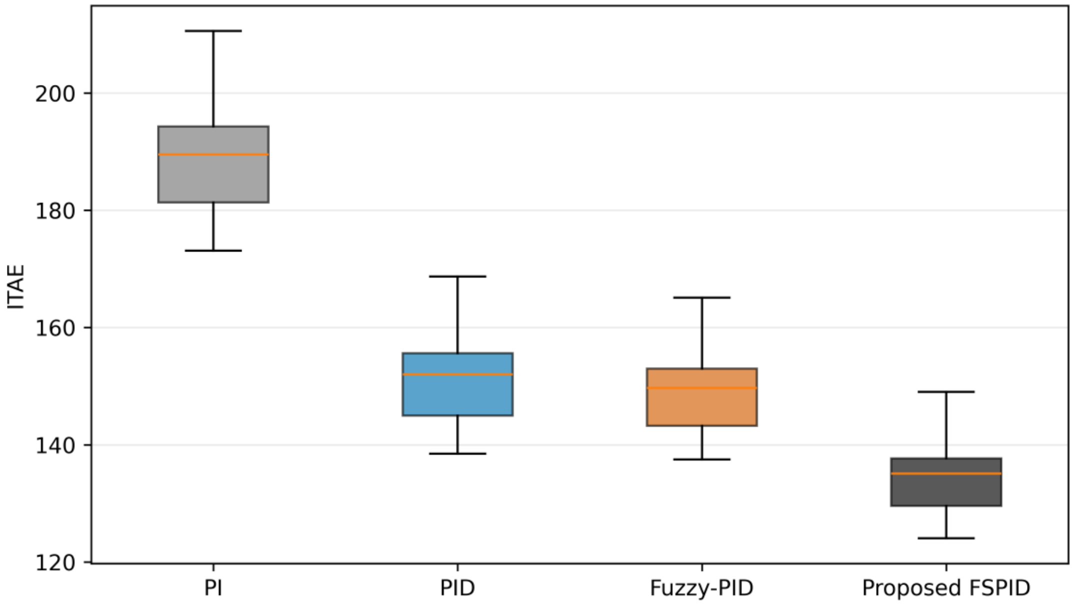

Fig. 7. ITAE distribution over 30 parameter-uncertainty and measurement-noise runs.

D. Interpretation and limitations

The results show where fuzzy supervision is helpful. Large error and error-rate combinations are contained in step changes, deep irradiance ramps, and PV loss. During these intervals the supervisor increases proportional and derivative action while moderating integral action. Integral authority returns when the disturbance edge has passed. This sequence reduces the first excursion and the late error tail. A direct fuzzy-PID with only one activation variable is not able to separate these phases as much, this is the reason of the less improvement when compared to the fixed PID.

The model is intentionally simple. It does not include elastic water-hammer waves, cavitation, backlash, turbine-efficiency maps, penstock resonance, converter current limits, sensor delay, communication loss, The 30-run study varies only inertia, turbine time constant, load damping and measurement noise. The paper is therefore not claimed to be ready for immediate commissioning. A credible next step would be to identify plant parameters, embed the proposed law in a high-fidelity waterway model, verify worst case gate rate and pressure rise, and proceed thru processor-in-the-loop, hardware-in-the-loop, and staged isolated-operation tests. Appropriate higher-fidelity comparators for that stage are provided by recent nonlinear hydro studies [18]-[22], [25]-[30].

V. CONCLUSION

In this paper, a bounded fuzzy-supervised PID governor for an isolated hydro-PV system is proposed. The approach modifies the three PID gains on-line, but retains the engineering structure required for implementation: filtered derivative, conditional anti-windup, gate saturation and explicit gain limits. The assessment is performed for 4 disturbance cases and 30 uncertain plant realizations. The proposed method has the lowest IAE, ISE, ITSE, ITAE and peak frequency deviation in all deterministic cases compared with PI, fixed PID and direct fuzzy-PID. It also keeps the minimum value of ITAE mean and standard deviation under parameter uncertainty and measurement noise. The improvement is thus consistent and not related to a favorable load step. Future work will include elastic waterway dynamics, rate limits, inverter frequency support, formal switched/nonlinear stability analysis, and real-time experimental validation.

REFERENCES

[1] C. Wang, D. Wang, and J. Zhang, “Experimental study on isolated operation of hydro-turbine governing system of Lunzua hydropower station in Zambia,” Renewable Energy, vol. 180, pp. 1237-1247, 2021. https://doi.org/10.1016/j.renene.2021.09.014

[2] G. Martínez-Lucas, J. I. Sarasúa, A. Fernández-Guillamón, and Á. Molina-García, “Combined hydro-wind frequency control scheme: Modal analysis and isolated power system case example,” Renewable Energy, vol. 180, pp. 1056-1072, 2021. https://doi.org/10.1016/j.renene.2021.09.002

[3] R. Alayi, F. Zishan, S. R. Seyednouri, R. Kumar, M. H. Ahmadi, and M. Sharifpur, “Optimal load frequency control of island microgrids via a PID controller in the presence of wind turbine and PV,” Sustainability, vol. 13, art. 10728, 2021. https://doi.org/10.3390/su131910728

[4] A. H. Yakout, H. Kotb, H. M. Hasanien, and K. M. AboRas, “Optimal fuzzy PIDF load frequency controller for hybrid microgrid system using marine predator algorithm,” IEEE Access, vol. 9, pp. 54220-54232, 2021. https://doi.org/10.1109/ACCESS.2021.3070076

[5] A. Naderipour et al., “Load-frequency control in an islanded microgrid PV/WT/FC/ESS using an optimal self-tuning fractional-order fuzzy controller,” Environmental Science and Pollution Research, 2021. https://doi.org/10.1007/s11356-021-14799-1
[6] S. Rawat, R. K. Saket, and C. K. Shiva, “Interval type-2 fuzzy logic control-based frequency stabilization of hybrid power system,” Applied Sciences, vol. 11, art. 10217, 2021. https://doi.org/10.3390/app112110217
[7] K. Rajagopal et al., “Coexisting attractors in a fractional-order hydro-turbine governing system and fuzzy PID-based chaos control,” Asian Journal of Control, vol. 23, pp. 894-907, 2021. https://doi.org/10.1002/asjc.2261
[8] A. Fernández-Guillamón et al., “Frequency control studies: A review of power system, conventional and renewable generation plant models,” Electric Power Systems Research, vol. 211, art. 108191, 2022. https://doi.org/10.1016/j.epsr.2022.108191
[9] F. Zishan et al., “Efficient PID control design for frequency regulation in an independent microgrid,” Electronics, vol. 11, art. 3886, 2022. https://doi.org/10.3390/electronics11233886
[10] M. A. Kamarposhti, H. Shokouhandeh, M. Alipur, I. Colak, H. Zare, and K. Eguchi, “Optimal designing of fuzzy-PID controller in the load-frequency control loop of hydro-thermal power system connected to wind farm by HVDC lines,” IEEE Access, vol. 10, pp. 63812-63822, 2022. https://doi.org/10.1109/ACCESS.2022.3183155
[11] M. Ali, H. Kotb, K. M. AboRas, and H. M. Hasanien, “Frequency regulation of hybrid multi-area power system using wild horse optimizer based new combined fuzzy fractional-order PI and TID controllers,” Alexandria Engineering Journal, vol. 61, 2022. https://doi.org/10.1016/j.aej.2022.06.008
[12] Y. N. Bulatov, A. V. Kryukov, and K. V. Suslov, “Group predictive voltage and frequency regulators for small hydro power plant in the context of low power quality,” Renewable Energy, vol. 200, pp. 571-578, 2022. https://doi.org/10.1016/j.renene.2022.10.017
[13] H. H. Coban, “Load frequency control of microgrid system by battery and pumped-hydro energy storage,” Water, vol. 14, art. 1818, 2022. https://doi.org/10.3390/w14111818
[14] M. Mokhtar et al., “An adaptive load frequency control for power systems with renewable energy sources,” Energies, vol. 15, art. 573, 2022. https://doi.org/10.3390/en15020573
[15] A. Fathy et al., “A new fractional-order load frequency control for multi-area power systems,” Sustainability, vol. 14, art. 14999, 2022. https://doi.org/10.3390/su142214999
[16] A. Bakeer et al., “Optimal ultra-local model control integrated with load frequency control of microgrids,” Energies, vol. 15, art. 9177, 2022. https://doi.org/10.3390/en15239177
[17] D. V. Doan, K. Nguyen, and Q. V. Thai, “Load-frequency control of three-area interconnected power systems with renewable energy sources using novel PSO-PID-like fuzzy logic controllers,” Engineering, Technology & Applied Science Research, vol. 12, pp. 8597-8604, 2022. https://doi.org/10.48084/etasr.4924
[18] F. Dao, Y. Zou, Y. Zeng, J. Qian, and X. Li, “An intelligent CPSOGSA-based mixed H2/H∞ robust controller for the multi-hydro-turbine governing system with sharing common penstock,” Renewable Energy, vol. 206, pp. 481-497, 2023. https://doi.org/10.1016/j.renene.2023.01.052
[19] Y. Zou et al., “Design of intelligent nonlinear robust controller for hydro-turbine governing system based on state-dynamic-measurement hybrid feedback linearization method,” Renewable Energy, vol. 204, pp. 635-651, 2023. https://doi.org/10.1016/j.renene.2023.01.019
[20] Z. Wu, Z. Wu, F. Kong, and H. Zhang, “Multi-objective feedback nonlinear sliding-mode control strategy based integrated regulator for hydropower set with sloping ceiling tailrace tunnel,” IEEE Access, vol. 11, pp. 18234-18244, 2023. https://doi.org/10.1109/ACCESS.2023.3246997
[21] P. C. Sahu et al., “A robust DQN-based grade-2 fuzzy cascaded controller for frequency regulation of islanded microgrid,” e-Prime—Advances in Electrical Engineering, Electronics and Energy, vol. 6, art. 100288, 2023. https://doi.org/10.1016/j.prime.2023.100288
[22] F. Amiri et al., “Improved load frequency control in power systems using an optimized fuzzy PID controller,” Algorithms, vol. 16, art. 539, 2023. https://doi.org/10.3390/a16120539
[23] S. B. Masikana, G. Sharma, and S. Sharma, “Renewable energy sources integrated load frequency control of power system: A review,” e-Prime—Advances in Electrical Engineering, Electronics and Energy, vol. 8, art. 100605, 2024. https://doi.org/10.1016/j.prime.2024.100605
[24] A. Hassan et al., “A comprehensive review of frequency response and frequency support from solar photovoltaic systems,” Renewable and Sustainable Energy Reviews, art. 116324, 2025. https://doi.org/10.1016/j.rser.2025.116324
[25] A. Dev, G. Sarvaiya, B. Parmar, and U. Chauhan, “Frequency stabilization in microgrid with PV system based on maximum power extraction: A sliding-mode approach,” e-Prime—Advances in Electrical Engineering, Electronics and Energy, vol. 9, art. 100692, 2024. https://doi.org/10.1016/j.prime.2024.100692
[26] I. F. Davoudkhani et al., “Robust load-frequency control of islanded urban microgrid using 1PD-3DOF-PID controller,” Scientific Reports, vol. 14, 2024. https://doi.org/10.1038/s41598-024-64794-y
[27] E. Alipour et al., “Enhanced frequency control of a hybrid microgrid using optimized PID controller,” Scientific Reports, vol. 14, 2024. https://doi.org/10.1038/s41598-024-73233-x
[28] D. K. Gupta et al., “Fractional-order PID controller for load frequency control in an interconnected power system,” Results in Engineering, vol. 22, art. 102442, 2024. https://doi.org/10.1016/j.rineng.2024.102442
[29] J. Chen et al., “Intelligent robust control for nonlinear complex hydro-turbine regulation system based on a novel state-space equation and dynamic feedback linearization,” Energy, vol. 302, art. 131798, 2024. https://doi.org/10.1016/j.energy.2024.131798
[30] Z. Liu et al., “Suppression and analysis of low-frequency oscillation in hydropower unit regulation systems with complex water diversion systems,” Energies, vol. 17, art. 4831, 2024. https://doi.org/10.3390/en17194831
[31] W. Guo, L. Wang, and F. Qu, “Optimization of governor parameters for transient process of hydropower system with two turbine units sharing a super long headrace tunnel,” Energy Science & Engineering, vol. 12, pp. 3505-3523, 2024. https://doi.org/10.1002/ese3.1832
[32] F. Dao et al., “Design of a novel state-feedback robust H2/H∞ sliding-mode controller for a hydraulic turbine governing system,” Scientific Reports, vol. 14, art. 29083, 2024. https://doi.org/10.1038/s41598-024-79493-x
[33] E. Wang et al., “Load frequency optimal control of the hydropower-photovoltaic hybrid microgrid system based on the off-policy integral reinforcement learning algorithm,” Frontiers in Energy Research, vol. 12, art. 1464722, 2024. https://doi.org/10.3389/fenrg.2024.1464722
[34] D. Liu, S. Zhao, and J. Zhang, “Adaptive PID control of hydropower units based on particle swarm optimization and fuzzy inference,” Water, vol. 17, art. 1512, 2025. https://doi.org/10.3390/w17101512
[35] J. Zhang et al., “Design of improved internal mode controller for hydro-turbine governing system based on generalized inverse solver method,” Scientific Reports, vol. 15, art. 19031, 2025. https://doi.org/10.1038/s41598-025-98223-5

[36] Y. Li et al., “Multi-objective optimized fuzzy fractional-order PID control for frequency regulation in hydro-wind-solar-storage systems,” Water, vol. 17, art. 2553, 2025. https://doi.org/10.3390/w17172553
[37] S. A. Zaid and K. S. Alatawi, “Implementation of fuzzy PID controller to an isolated wind/battery/super magnetic energy storage power system,” Processes, vol. 13, art. 515, 2025. https://doi.org/10.3390/pr13020515